Applied Nanoscience (2020) 10:5219–5232
https://doi.org/10.1007/s13204-020-01400-3

ORIGINAL ARTICLE

Chemically reactive swirling flow of viscoelastic nanofluid due to rotating disk with thermal radiations

Masood Khan[1] · Jawad Ahmed[1,2] · Wajid Ali[1] · Sohail Nadeem[3,4]

Received: 16 January 2020 / Accepted: 10 April 2020 / Published online: 3 May 2020

Abstract
Researchers and engineers working in the field of thermal analysis are in the pursuit of innovative methods to improve the performance of energy devices by enhancing their thermal characteristics. Aimed at this purpose, the fluid flow investigation comprising of nanoparticles is supposed to be one of the best significant procedures for augmenting heat transfer systems. The current study describes the investigation of Buongiorno model for the evaluation of transient flow and heat transfer of Maxwell nanofluids over a rotating and vertically moving disk. The significant impact of Lorentz forces due to the interaction of magnetic field applied vertically on Maxwell fluid is also investigated. Additionally, the chemical reaction and thermal radiation effects have been discussed on heat and mass transfer mechanisms. Furthermore, Brownian motion and thermophoresis characteristics are studied due to nanofluids. With the help of similar transformations, the equations of motion are simplified into a set of a nonlinear system of ordinary differential equations. The solution of the problem is presented via numerical technique, namely bvp4c in Matlab. The numerical outcomes are illustrated through graphical and tabular forms. It is observed that the upward and downward motion of the disk exert similar effects to that of the injection/suction through the wall. The boundary layer thickness of temperature and concentration fields are enhanced due to the presence of thermophoresis force. The impact of Lorentz force is to reduce the radial and azimuthal velocities and increase the temperature of nanofluid. Furthermore, it is noticed that the concentration profile reduces with the thermophoresis effect and Schmidt number.

Keywords Rotating disk · Maxwell nanofluid · Buongiorno model · Radiative flow · Numerical solutions

Abbreviations

r, φ, z	Cylindrical coordinate system
u, v, w	Velocity components
ρ	Fluid density
Sh_r	Local Sherwood number
ϕ	Dimensionless concentration
p, T	Fluid pressure and temperature
F	Dimensionless radial velocity
G	Dimensionless azimuthal velocity
H	Dimensionless axial velocity
ν, μ	Kinematic and dynamic viscosities
λ_1	Relaxation time parameter
$C_w(t)$	Wall concentration
k^*	Mean absorption coefficient
C_∞	Ambient concentration
δ	Boundary layer thickness
α_1	Wall temperature parameter
$a(t)$	Vertical distance
Nt	Thermophoresis parameter
ω	Rotation parameter
D_B	Brownian diffusion coefficient
α	Thermal diffusivity
Re	Reynolds number
S	Wall motion
c_p	Specific heat at constant pressure
ρc_p	Heat capacity of fluid
η	Dimensionless variable
θ	Dimensionless temperature
Nu_r	Local Nusselt number

✉ Sohail Nadeem
sohail.nadeem@tdtu.edu.vn

1 Department of Mathematics, Quaid-i-Azam University, Islamabad 44000, Pakistan

2 Department of Basic Sciences, University of Engineering and Technology, Taxila 47050, Pakistan

3 Mathematics and its Applications in Life Sciences Research Group, Ton Duc Thang University, Ho Chi Minh, Vietnam

4 Faculty of Mathematics and Statistics, Ton Duc Thang University, Ho Chi Minh, Vietnam

c, Ω	Stretching and rotation rate constants
Pr	Prandtl number
β_1	Deborah number
q_{rad}	Radiative heat flux
c_f	Fluid density and specific heat
$T_w(t)$	Wall temperature
T_∞	Ambient fluid temperature
α_2	Wall concentration parameter
σ^*	Stefan–Boltzmann constant
Nb	Brownian motion parameter
Rd	Radiation parameter
D_T	Thermophoresis diffusion

Introduction

The heat transfer mechanisms are important due to the efficiency of many technological and industrial applications. Over the decade, the scientists and engineers are taking advantages of nanofluid technology, to achieve the required goal. The term "nanofluid" was first proposed by Choi and Eastman (1995). Recently, the practical applications of nanofluid in heat transfer equipment include radiators, heat exchanger, solar collectors, electronic cooling system, detergency, automobile, and medical applications. Temperature plays an important role in increasing the effect of thermal conductivity of nanofluid. However, the performance of the thermal conductivity depends on size, shape, and material of nanofluid. For example, metallic nanofluid have higher thermal conductivity than non-metallic nanofluid and the small-sized nanoparticle has higher thermal conductivity as compared to the large-sized nanoparticles. The temperature effects on the thermal conductivity have been studied in Refs. Das et al. (2003), Chon and Kihm (2005), and Li and Peterson (2006). The features of two slip mechanisms called Brownian diffusion and thermophoresis were studied by Buongiorno (2006). These two features of nanofluid create enhanced heat transfer effects which were presented by Sheikholeslami et al. (2014). Heat transfer in nanofluid flow over a flat plate with the help of self-similar transformations was given by Avramenko et al. (2014). The three-dimensional flow of nanofluid due to stationary or moving surface was presented by Khan et al. (2014). Hayat et al. (2015) proposed the model for magnetohydrodynamic (MHD) three-dimensional flow over a couple of stress nanofluid in the presence of nonlinear thermal radiation over a stretchable surface. The stagnation point of the rotating nanofluid in boundary layer flow on the external surface was given by Anwar et al. (2015). The nanofluid flow between two parallel plates in the presence of a magnetic field was studied by Sheikholeslami et al. (2016). Mustafa (2017) studied the Buongiorno model of nanofluid flow due to a rough rotating disk. Khan et al. (2018) discussed the nanofluid flow over a rotating disk under the influence of magnetic field and dissipation effects. The effects of chemically reaction, magnetic field and heat source on Sutterby nanofluid flow due to rotating stretchable disk were examined by Hayat et al. (2018). The motion of nanofluid thin film on a rotating disk under the influence of non-linear thermal radiation was studied by Ahmed et al. (2019). Some recent articles on nanofluids are given in Refs. Turkyilmazoglu (2016), Turkyilmazoglu (2019a, b), Ahmed et al. (2019a, b, c), and Turkyilmazoglu (2020).

The heat transfer flow problem over a rotating disk has numerous practical applications in various engineering applications such as rotating machinery, gas turbine rotator, air cleaning machines, thermal power generating systems, computer storage devices, and electronic devices. The current problem also discusses the heat transfer flow over rotating disk in the presence of nanofluid, which is a quite interesting topic in recent literature. At very first in 1920, Karman (1921) presented the problem for rotating disk to the case of flow impulsively starting from rest. Following the pioneering work of Karman, many new problems have been introduced to the rotating disk flow problem, e.g., the surface of rotating disk having suction/injection properties was studied in Stuart (1954) and Kuiken (1971). The transfer of heat from an air-cooled rotating disk was proposed by Owen et al. (1974). Hall (1986) and Jarre et al. (1996) have studied the aspects of rotating disk problem theoretically, numerically and experimentally. The characteristics of flow and heat transfer due to rotating disk was presented by Turkyilmazoglu (2014). Khan et al. (2020a, b) presented the Maxwell fluid model for rotating and vertically moving disk by analyzing flow features, MHD and non-linear thermal radiation over a rotating disk.

Fluids such as water, oil, and air are classified as Newtonian fluids, while the non-Newtonian fluids are honey, blood, paint polymer solution, corn starch in water, ketchup, motor oil, lubricant spray, coffee in water and hydraulics fluids. However, in many industrial process of fluid motion, we have to deal with non-Newtonian fluids, due to the fact that various assumptions of Newtonian behavior are not valid. In general terms "non-Newtonian" is related as viscoelastic. Non-Newtonian can be defined as the dependence of its viscosity to the stress applied but this does not mean that all non-Newtonian fluids need to have elastic properties. There are some examples of inelastic behavior, i.e. shear stress dependence on viscosity in Bird et al. (1977). Ezzat (2010) investigated the conducting thermoelectric materials for a new class of thermoelectric non-Newtonian fluids. The applications and perspective of non-Newtonian fluids in industries were given by Peng et al. (2014). Nadeem et al. (2014) investigated a model of non-Newtonian nanofluid over a stretchable sheet. The characteristic connection of non-Newtonian nanofluid between two vertical plates is investigated analytically and numerically by Hatami and Ganji (2014).

Radiative effects are important during the heat transfer process because they have many applications in engineering, industries, and material science, for instance, gas for a cooled reactor, glass production, furnace design, polymer preparing, in space technology, etc. Furthermore, electromagnetic waves are responsible for transfer heat and energy via radiations. However, there is no attempt in the literature to consider the radiation effects on flow and heat transfer of Maxwell nanofluid over a vertically moving rotating disk. Radiation effects on free convection viscous incompressible flow past a vertical porous plate with uniform temperature and suction were analyzed by Hossain et al. (1999). Some investigations regarding the effects of thermal radiation using linearized Rosseland approximation are given in Refs. Ellahi et al. (2016), Akbar et al. (2016), Alebraheem and Ramzan (2019), Ellahi et al. (2019), Alamri et al. (2019), Sarafraz et al. (2020), and Ellahi et al. (2020). Effects of thermal radiation in the peristaltic flow of Jeffrey nanofluid and MHD nanofluid flow are discussed by Hayat et al. (2016, 2015).

The aim of the present work is to investigate the effects of non-linear thermal radiation on the flow and temperature fields across an unsteady MHD nanofluid over a vertically moving disk. Buongiorno's model is implemented for the current analysis to show the impact of Brownian motion and thermophoresis due to nanoparticles. Using Karman transformation variables, the motion equations are integrated numerically for solution through the built-in scheme, namely *bvp4c* in MATLAB. Graphical behavior is presented to describe the role of physical parameters. Such as wall motion, magnetic parameter, Deborah number, and Schmidt number.

Mathematical modeling

The graphical view of rotating and vertically moving disk geometry is shown in Fig. 1. We consider an incompressible Maxwell nanofluid over a rotating and vertically moving disk. The physical problem is associated with the cylindrical coordinates $(r,\ \varphi,\ z)$ with the directions of radial, azimuthal and axial as $(u,\ v,\ w)$, respectively. A uniform beam of magnetic field is thrown along the z-axis. A well-known Buongiorno's model is implemented to trace the features of thermophoresis and Brownian diffusion. Furthermore, the disk is rotating as well as vertically moving so we have an ambient temperature T_∞ and concentration C_∞ of fluid, whereas the disk is subjected to the time-dependent wall temperature $T_w(t)$ and time-dependent wall concentration $C_w(t)$. So this will make the difference in temperature and concentration. Temperature and concentration difference are given as

$$\Delta T = T_w(t) - T_\infty,\ \Delta C = C_w(t) - C_\infty. \tag{1}$$

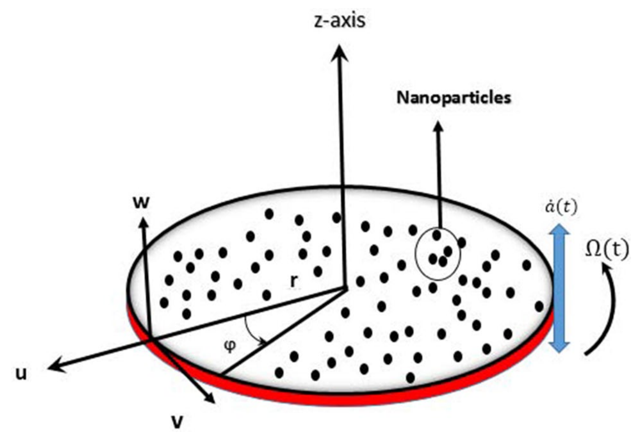

Fig. 1 Flow configuration

The expressions for wall temperature (Turkyilmazoglu 2018) and concentration are given as

$$T_w(t) = \mathrm{c}a(t)^{-2\alpha_1} + T_\infty,\ C_w(t) = \mathrm{c}a(t)^{-2\alpha_2} + C_\infty, \tag{2}$$

where c is the arbitrary constant and α_1 and α_2 are the wall temperature and wall concentration parameters, respectively. When $\alpha_1 = \alpha_2 = 0$, then the wall is sustained a constant wall temperature and constant wall concentration.

These assumptions lead to the following flow problem (Ahmed et al. 2019b):

$$u_r + \frac{u}{r} + w_z = 0, \tag{3}$$

$$\begin{aligned} &u_t + uu_r + wu_z - \frac{v^2}{r} + \lambda_1 \\ &\left(\begin{array}{c} u^2u_{rr} + u_{tt} + 2uu_{rt} + 2wu_{zt} - 2\frac{v}{r}v_t - \frac{2vu}{r}v_r + \frac{v^2u}{r^2} - \frac{2wv}{r}v_z \\ +2wuu_{rz} + w^2u_{zz} + \frac{v^2}{r}u_r \end{array} \right) \\ &= \nu\left\{u_{zz}\right\} - \frac{\sigma B_o^2}{\rho f}\left(u + \lambda_1\left(u_t + wu_z\right)\right), \end{aligned} \tag{4}$$

$$\begin{aligned} &v_t + wv_z + uv_r + \frac{vu}{r} + \lambda_1 \\ &\left(\begin{array}{c} u^2v_{rr} + w^2v_{zz} + v_{tt} + 2uv_{rt} + 2\frac{v}{r}u_t + 2wv_{zt} - \frac{2vu^2}{r^2} + \frac{2vu}{r}u_r - \frac{v^3}{r^2} \\ +2uwv_{rz} + \frac{2wv}{r}u_z + \frac{v^2}{r}v_r \end{array} \right) \\ &= \nu\left\{v_{zz}\right\} - \frac{\sigma B_o^2}{\rho f}\left(v + \lambda_1\left(v_t + wv_z\right)\right), \end{aligned} \tag{5}$$

$$\begin{aligned} &T_t + uT_r + wT_z + \frac{1}{\rho c_p}(q_{rad})_z \\ &= \alpha\left\{T_{zz}\right\} + \tau\left(D_BT_zC_z + \frac{D_T}{T_\infty}\left(T_z\right)^2\right), \end{aligned} \tag{6}$$

$$C_t + uC_r + wC_z = \frac{D_T}{T_\infty}\left(T_{zz}\right) + D_B\left(C_{zz}\right), \tag{7}$$

where the subscripts involving either of the variables r, z, and t represent the partial derivatives. Further (u, v, w) show the velocity components, (C, T) concentration and temperature, respectively, τ shows the heat capacities of ratio. (D_B, D_T) denote the Brownian diffusion and thermophoresis diffusion coefficients. With the help of Rosseland approximation, the radiative heat flux q_{rad} in Eq. (6) can be written as Ahmed et al. (2019b)

$$q_{\text{rad}} = -\frac{4\sigma^*}{3k^*}\left(T_z^4\right) = -\frac{16\sigma^* T^3}{3k^*}T_z. \tag{8}$$

In the above expressions, k^* and σ^* are denoted as mean absorption coefficient and Stefan–Boltzmann constant. Using Eq. (8) in Eq. (6), we get

$$\begin{aligned} &T_t + uT_r + wT_z - \frac{16\sigma^*}{3\rho c_p k^*}\left(T^3 T_z\right)_{,z} \\ &\quad = \alpha\left(T_{zz}\right) + \tau\left(D_B T_z C_z + \frac{D_T}{T_\infty}\left(T_z\right)^2\right). \end{aligned} \tag{9}$$

Boundary conditions

The physical problem is modeled under the following conditions (Turkyilmazoglu 2018):

$$\begin{aligned} &u = 0,\ v = \Omega(t)r,\ w = \beta\dot{a}(t),\ C = C_w(t), \\ &T = T_w(t) \text{ at } z = a(t), \\ &u = v = 0,\ C = C_\infty,\ T = T_\infty \text{ as } z \to \infty, \end{aligned} \tag{10}$$

where β is the strength of wall porosity. The constant value of $\beta = 1$ implies $w = \dot{a}(t)$ which means the moving surface is impermeable having no heat and mass transfer workout. As we are discussing the action of wall motion, the strength of wall porosity is either wall suction or wall injection. Here we classified the wall injection for the value $\beta > 1$ and for the wall suction $\beta < 1$. In the current study, the wall strength is set to be fixed with $\beta = 2$.

Similarity hypothesis

We define the following transformations (Hayat et al. 2015):

$$\begin{aligned} &(u,\ v,\ w,\ T,\ C) \\ &\quad = \left(F\frac{rv}{a^2(t)},\ G\frac{rv}{a^2(t)},\ H\frac{v}{a(t)},\ T_\infty + \Delta T\theta,\ C_\infty + \Delta C\phi\right), \\ &\left(\eta,\ \eta_t,\ \eta_z\right) = \left(\frac{z}{a(t)} - 1,\ -\frac{\dot{a}(t)}{a(t)}(\eta+1),\ \frac{1}{a(t)}\right), \end{aligned} \tag{11}$$

where η is the non-dimensional distance measured along the axis of rotation, F, G and H are the radial velocity, tangential velocity and axial velocity, respectively, and these are the functions of η. Using Eq. (11) in Eqs. (3–5), (7), (9) and (10), we obtain

$$2F + H' = 0, \tag{12}$$

$$\begin{aligned} &F'' - F^2 + G^2 - HF' + S(1 - S\beta_1)\left(F + \frac{\eta+1}{2}F'\right) \\ &\quad - \frac{3}{2}S^2\beta_1\left(F + (\eta+1)F' + \frac{(\eta+1)^2}{6}F''\right) \\ &\quad + 2\beta_1(2HGG' - 2HFF' + H^2F'') \\ &\quad - M\left(F - S\beta_1(F + \frac{\eta+1}{2}F') + \beta_1 HF'\right) + 2S\beta 1 \\ &\quad \left(HF + F^2 - G^2 + \frac{(\eta+1)}{2}\left(FF' + GG' + HF''\right)\right) \\ &\quad = 0, \end{aligned} \tag{13}$$

$$\begin{aligned} &G'' - 2FG - HG' + S\left(1 - S\beta_1\right)\left(\frac{\eta+1}{2}G' + G\right) \\ &\quad - \frac{3}{2}S^2\beta_1\left(G + (\eta+1)G' + \frac{(\eta+1)^2}{6}G''\right) \\ &\quad - 2\beta_1\left(2FHG' + 2HGF' + H^2G''\right) \\ &\quad - M\left(G - S\beta_1\left(G + \frac{\eta+1}{2}G'\right) + \beta_1 HG'\right) \\ &\quad + 2S\beta_1\left(2FG' + HG' + \frac{(\eta+1)}{2}\left(GF' + FG' + HG''\right)\right) \\ &\quad = 0, \end{aligned} \tag{14}$$

$$\begin{aligned} &\left(1 + \frac{4}{3}\text{Rd}\right)\theta'' \\ &\quad + \frac{4}{3}\text{Rd}\left[\begin{array}{c} \left(\theta_w - 1\right)^3\left(3\theta^2\theta'^2 + \theta^3\theta''\right) + 3\left(\theta_w - 1\right)^2\left(2\theta\theta'^2 + \theta^2\theta''\right) \\ +3\left(\theta_w - 1\right)\left(\theta'^2 + \theta\theta''\right) \end{array}\right] \\ &\quad + \Pr S\left(\alpha_1\theta + \frac{\eta+1}{2}\theta'\right) \\ &\quad + \Pr\left(\text{Nb}\theta\phi' + \text{Nt}\theta'^2 - H\theta'\right) = 0, \end{aligned} \tag{15}$$

$$\phi'' - \mathrm{Sc}H\phi' + \frac{\mathrm{Nt}}{\mathrm{Nb}}\theta'' + \mathrm{Sc}\,S\left[\alpha_2\phi + \frac{\eta+1}{2}\phi\right] = 0, \tag{16}$$

$$\begin{aligned} &F(0) = 0,\ G(0) = \omega,\ H(0) = \beta\frac{S}{2},\ \theta(0) = 1 = \phi(0), \\ &F(\infty) = G(\infty) = \theta(\infty) = \phi(\infty) = 0. \end{aligned} \tag{17}$$

In the above equations, $F,\ G,\ H,\ \theta$, and ϕ are the dimensionless radial, azimuthal and axial velocities, temperature and concentration parameter, respectively. From Eqs. (12–17), there are some parameters that influence the flow motion, temperature and concentration fields of Maxwell nanofluid. These are $S,\ \beta_1$, Nt, Nb, β, Rd, θ_w, M, ω, Pr, α_1, α_2, and Sc, respectively, called wall motion up and down, Deborah number, thermophoresis, Brownian motion, wall permeability, radiation parameter, temperature ratio parameter, magnetics field, rotation parameter, Prandtl number, wall temperature parameter, wall concentration parameter, and Schmidt numbers. The mathematical forms of these parameters are

$$\begin{aligned} &S = \frac{2a(t)\dot{a}(t)}{\nu},\ a(t) = h\sqrt{\frac{S\nu}{h^2}t + 1},\ \ \beta_1 = \frac{\lambda_1\nu}{a^2(t)}, \\ &\mathrm{Nt} = \frac{\tau D_B c a(t)^{-2\alpha_1}}{\tau_0\nu},\ \mathrm{Nb} = \frac{\tau D_B c a(t)^{-2\alpha_2}}{\nu}, \\ &R_d = \frac{4\sigma^* T_\infty^3}{3kk^*},\ M = \frac{\sigma B_0^2 a^2(t)}{\nu\rho_f},\ \omega = \frac{\Omega(t)\, a^2(t)}{\nu}, \\ &\mathrm{Pr} = \frac{\nu}{\alpha},\ S_c = \frac{\nu}{D_B}. \end{aligned} \tag{18}$$

Here $\Omega(t) = \frac{\omega\nu}{h^2+\nu St}$ implies the rotation of disk. The value $S > 0$ reduces the rotation of disk and thus causing disk decelerating rotation. Contrarily, $S < 0$ enhances the rotation of disk which accelerates the rotation of disk.

Nusselt number

From the engineering perspective, the quantity local Nusselt number Nu_r is very important. Physically, Nu_r is the wall heat transfer. This is expressed by the following expression:

$$\mathrm{Nu}_r = -\left[1 + \frac{16\sigma^* T_\infty^3}{3\rho c_p k^*}\right]\frac{r}{(T_w - T_\infty)}\left(\frac{\partial T}{\partial z}\right)|_{z=0}\,. \tag{19}$$

In dimensionless notation, one can write

$$\begin{aligned} &\mathrm{Re}^{-1/2}\,Nu_r \\ &\quad = -\theta'(0)\left(1 + \frac{4}{3}\mathrm{Rd}\left\{1 + \theta(0)(\theta_w - 1)\right\}^3\right), \end{aligned} \tag{20}$$

where $\mathrm{Re}^{1/2} = \frac{r}{a(t)}$ is the local Reynolds number.

Sherwood number

Mass transfer rate at the disk surface can be defined through Sherwood number as follows:

$$\mathrm{Sh}_r = -\frac{r}{(C_w - C_\infty)}\left(\frac{\partial C}{\partial z}\right)|_{z=0,} \tag{21}$$

and dimensionless form is

$$\mathrm{Sh}_r\mathrm{Re}^{-\frac{1}{2}} = -\phi'(0). \tag{22}$$

Numerical solution procedure

The numerical solution of the dimensionless nonlinear momentum, temperature, and concentration Eqs. (12–16) with the boundary conditions (17) are computed numerically with the bvp4c technique, one of the collection methods which uses the Lobatto formula. This technique requires initial guesses which satisfy the boundary conditions. Once initial guesses are provided by user then another built-in method, namely finite difference method is used to modify the guesses for further iterations. The order of accuracy in the numerical calculation is controlled with error tolerance less 10^{-6}. By default, this collocation method uses 61 grid points with CPU time of 12 s. In this process, we convert higher order system of ordinary differential equations into a system of first-order ordinary differential equations by introducing some new variables defined as

$$\begin{aligned} &H = X_1,\ H' = X_1',\ F = X_2,\ F' = X_3,\ F'' = X_3', \\ &G = X_4,\ G' = X_5, \\ &G'' = X_5',\ \theta = X_6,\ \theta' = X_7,\ \theta'' = X_7',\ \phi = X_8, \\ &\phi' = X_9,\ \phi'' = X_9'. \end{aligned} \tag{23}$$

$$X_1' = -2X_2, \tag{24}$$

$$X_3' = \frac{\begin{array}{c} X_2^2 - X_4^2 + X_1X_3 + S(S\beta_1 - 1)\left(X_2 + \frac{\eta+1}{2}X_3\right) + \frac{3}{2}S^2\beta_1(X_2 + (\eta+1)X_3) \\ -2S\beta_1\left(X_2^2 - X_4^2 + X_1X_2 + \frac{\eta+1}{2}(X_2X_3 + X_4X_5)\right) - 4\beta_1(X_1X_4X_5 - X_1X_2X_3) \\ +M\left(X_2 - S\beta_1\left(X_2 + \frac{\eta+1}{2}X_3\right) + \beta_1X_1X_3\right) \end{array}}{1 - \frac{S^2\beta_1}{4}(\eta+1)^2 + S\beta_1X_1(\eta+1) + 2\beta_1X_1^2}, \tag{25}$$

$$X_5' = \frac{\begin{array}{c}2X_2X_4 + X_1X_5 + S\left(S\beta_1 - 1\right)\left(X_4 + \frac{\eta+1}{2}X_5\right) + \frac{3}{2}S^2\beta_1\left(X_4 + (\eta+1)X_5\right)\\ -2S\beta_1\left(2X_2X_5 + X_1X_5 + \frac{\eta+1}{2}\left(X_2X_5 + X_4X_3\right)\right) + 4\beta_1\left(X_1X_2X_5 - X_1X_3X_4\right)\\ +M\left(X_4 - S\beta_1\left(X_4 + \frac{\eta+1}{2}X_5\right) + \beta_1X_1X_5\right)\end{array}}{1 - \frac{S^2\beta_1}{4}(\eta+1)^2 + S\beta_1X_1(\eta+1) + 2\beta_1X_1^2}, \tag{26}$$

$$X_7' = \frac{\begin{array}{c}\Pr\left(X_1X_7 - S\left(\frac{\eta+1}{2}X_7 + \alpha_1X_6\right)\right) - 4\mathrm{Rd}\left(\theta_w - 1\right)^3X_6^2X_7^2 - 8\mathrm{Rd}\left(\theta_w - 1\right)^2X_6X_7^2\\ -4\left(\theta_w - 1\right)X_7^2 - \Pr\left(NtX_7^2 + NbX_7X_9\right)\end{array}}{1 + \frac{4}{3}\mathrm{Rd} + \frac{4}{3}\mathrm{Rd}\left(\theta_w - 1\right)^3X_6^3 + 4\mathrm{Rd}\left(\theta_w - 1\right)^2X_6^2 + 4\mathrm{Rd}\left(\theta_w - 1\right)X_6} \tag{27}$$

$$X_9' = Sc\left(X_1X_9 - S\left(\frac{\eta+1}{2}X_9 + \alpha_2X_8\right)\right) - \frac{\mathrm{Nt}}{\mathrm{Nb}}X_7' \tag{28}$$

with conditions

$$\begin{aligned}&X_1(0) = \beta\frac{S}{2},\ X_2(0) = 0,\ X_4(0) = \omega,\\ &X_6(0) = 1 = X_8(0),\\ &X_2(\infty) = X_4(\infty) = X_6(\infty) = X_8(\infty) = 0.\end{aligned} \tag{29}$$

Code validation

The validation of numerical outcomes for local skin friction and Nusselt number is shown in Tables 1 and 2. Table 1 shows the comparison with Turkyilmazoglu (2018) for the effects of wall motion parameter S on local skin friction and Nusselt number by keeping other parameters $\omega = 1.0,\ \Pr = 1.0,\ \beta = 2$ and $\alpha_1 = 0.5$ fixed and rest of parameters zero. In Table 2, we have fixed the values $\omega = 2.0,\ \Pr = 1.0,\ \beta = 2$ and $\alpha_1 = 0.5$ and other parameters are zero. These tables show an excellent comparison and correlation with Turkyilmazoglu (2018).

Graphical discussion

In this section, we present the physical description and numerical simulation for the velocity, temperature and concentration fields, local Nusselt and Sherwood numbers for an unsteady Maxwell nanofluid flow. Heat transfer analysis is done with the consideration of Buongiorno's model. The graphical and numerical results are discussed with the parameters in the following ranges:

$$\begin{aligned}&S \in [-0.6,\ 0.4],\ M \in [0,\ 3.0],\ \mathrm{Nb} \in [0.3,\ 2.0],\\ &\mathrm{Nt} \in [0.0,\ 1.2],\ \Pr \in [0.5,\ 2.5],\\ &\beta_1 \in [0.0,\ 2.8],\ \mathrm{Rd} \in [0,\ 0.8],\ \theta_w \in [1, 2.2],\\ &\alpha_1 \in [-3,\ 1],\ \alpha_2 \in [1,\ 1.8]\end{aligned}$$

and fixing the values

$$\begin{aligned}&\beta = \omega = 2.0,\ S = M = \mathrm{Rd} = \beta_1 = 0.2,\ \theta_w = 1.2,\\ &\mathrm{Sc} = \alpha_1 = \alpha_2 = 1.0,\ \mathrm{Nt} = 0.4,\ \mathrm{Nb} = 0.6.\end{aligned}$$

Figure 2a shows the variation of radial velocity with the variation of wall motion S. It clearly shows that an upward wall motion reduces the rotational features of radial velocity. These effects on the rotating disk are blowing like for an upward action of wall motion. It is noted an enhancement in radial velocity with the action of wall motion. Similarly, Fig. 2b demonstrates the tangential velocity of nanofluid with varying values of wall motion parameter S. The influence of wall motion is to enhance the tangential velocity of nanofluid. The effects of wall motion parameter on the axial velocity show the blowing which increases the axial velocity of nanofluid as shown in Fig. 2c. In Fig. 2d, e, the effects of wall motion parameter on the temperature θ and concentration ϕ fields of the nanofluids are shown. It is obvious from these figures that both temperature and concentration profiles are increasing function of S.

Figure 3a–d illustrates the graphical behavior of fluid velocity and temperature field with the effects of Deborah number β_1. Deborah number is defined as the ratio of time relaxation to observation time. So progressing value of β_1 increases the relaxation time which indicates the more solid-like characteristics. $\beta_1 = 0$ implies the Maxwell fluid reduces into case of viscous fluid. Figure 3a, c shows the increase in quantity β_1, for which the reduction in radial and axial velocities of nanofluids is observed. In Fig. 3b–d, it is noted the effects of Deborah number is to increase

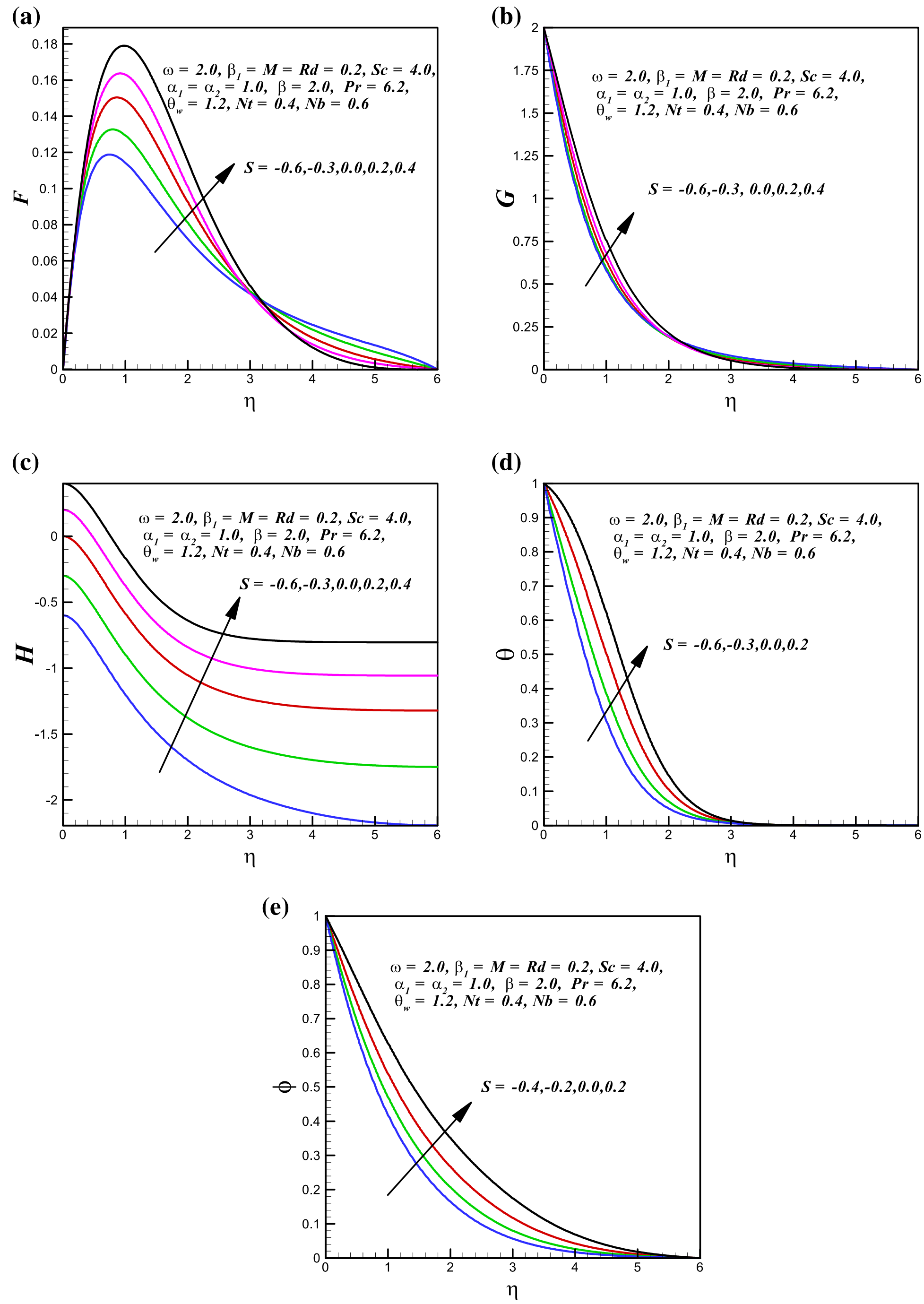

Fig. 2 Variation of S on **a** radial velocity, **b** azimuthal velocity, **c** axial velocity, **d** temperature profile and **e** concentration profile

the azimuthal velocity and temperature field of Maxwell nanofluid over vertically moving disk.

Figure 4a–d shows the effects of magnetic field parameter M. The features of magnetic field are tested on velocity field of nanofluid over vertically moving disk. It is observed that the higher magnetic field has the tendency to slow down the motion of nanofluid. Physically, the magnetic parameter M is ratio of the electromagnetic force to viscous force, so an increasing value of M implies the viscous force is dominant and as a result it decreases the radial and tangential velocity components. On the contrary it is noted that the axial velocity and temperature distribution enhance with the increase of magnetic field effects.

Figure 5a, b shows the variation of temperature field of nanofluids with the increasing effects of Brownian motion and thermophoresis parameter over vertically moving disk. Here both parameters Nt and Nb are showing a significant increase in temperature profile. This trend is expected because the properties of Brownian motion create the random motion in fluid that causes an increase in temperature

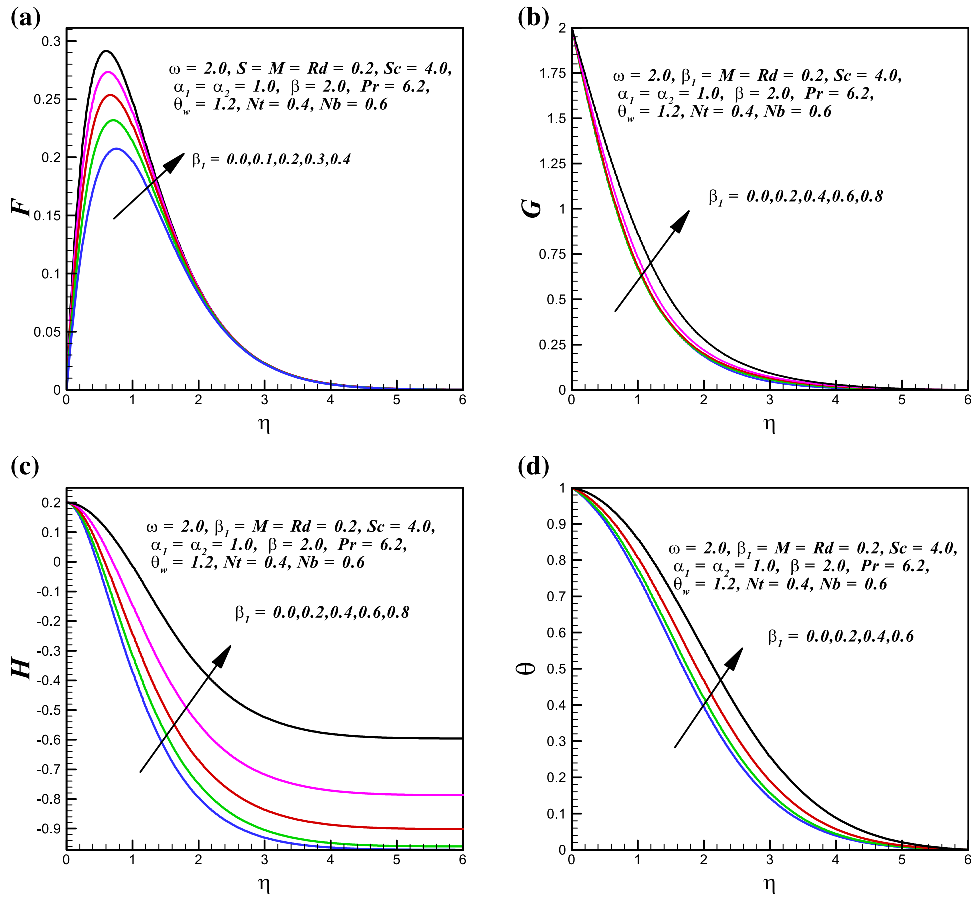

Fig. 3 Variation of β_1 on **a** radial velocity, **b** azimuthal velocity, **c** axial velocity, and **d** temperature profile

field of nanofluid. Figure 5c, d demonstrates the behavior of concentration field of Maxwell nanofluid with the variation of Brownian motion and thermophoresis. It is obvious that the Brownian motion creates random motion in fluid that creates resistance and consequently the concentration of fluids decreases with the Brownian motion effects. On the contrary, variation of concentration profile against the thermophoresis effect is shown in Fig. 5d. Physically, thermophoresis effects simply repel the particles away from a hot surface to cold surface due to which the concentration profile increases. The features of Nt are to enhance the concentration field.

Figure 6a, b shows the effects of radiation parameter Rd and Prandtl number Pr on temperature field of nanofluids. An increase in temperature as well as thermal boundary layer thickness of nanofluid with the gradual enhancement in Rd is observed. However, the trends of temperature field for Pr are quite opposite. Figure 6c, d displays the variation of temperature field θ with the effects of temperature ratio parameter θ_w and wall temperature parameter α_1. The temperature field of nanofluid enhances with both temperature ratio parameter θ_w and wall temperature parameter α_1. Figure 7a displays the variation of Schmidt number in the concentration profile. Concentration of fluid decreases due to decrease in mass diffusivity. Figure 7b shows the variation of wall concentration parameter in a concentration profile. It is seen that ϕ is an increasing function of α_2.

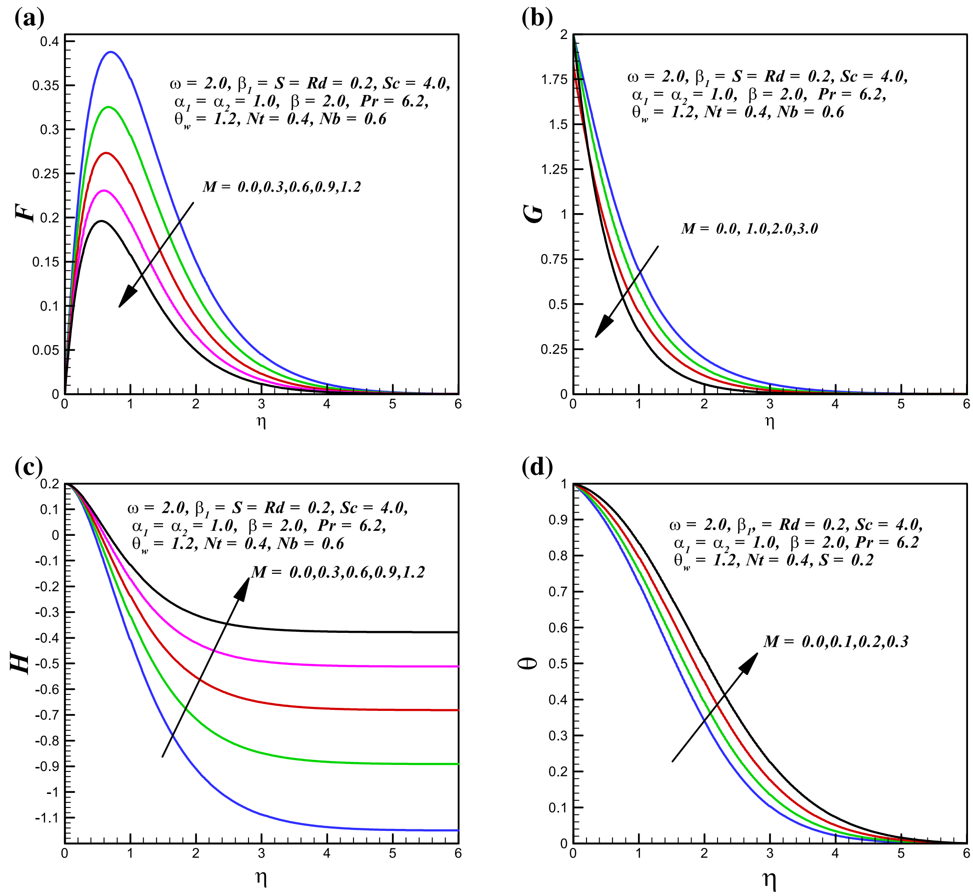

Fig. 4 Variation of M on **a** radial velocity, **b** azimuthal velocity, **c** axial velocity, and **d** temperature profile

Figure 8a, b shows the heat transfer rate with variation of parameters (Nt, S) and (ω, Rd). Figure 8a shows the decreasing behavior with increasing (Nt, S). Figure 8b illustrates an increase in heat transfer with increasing (ω, Rd). Figure 8c displays an increase in mass transfer with increasing wall motion parameter S. Figure 8d presents an increase in mass transfer rate with increasing the fluid thermophoresis Nt and Brownian motion Nb.

Concluding remarks

In this study, we have investigated the flow behavior during an unsteady motion of Maxwell nanofluid over vertically moving as well as rotating disk in the presence of magnetic field effects. The Buongiorno model is implemented to reveal the effects of Brownian motion and thermophoresis due to nanofluids. The impacts of some leading parameters on the flow behavior, temperature and concentration fields of nanofluids via graphical and tabular forms are discussed. The following significant features of this study can be summarized a

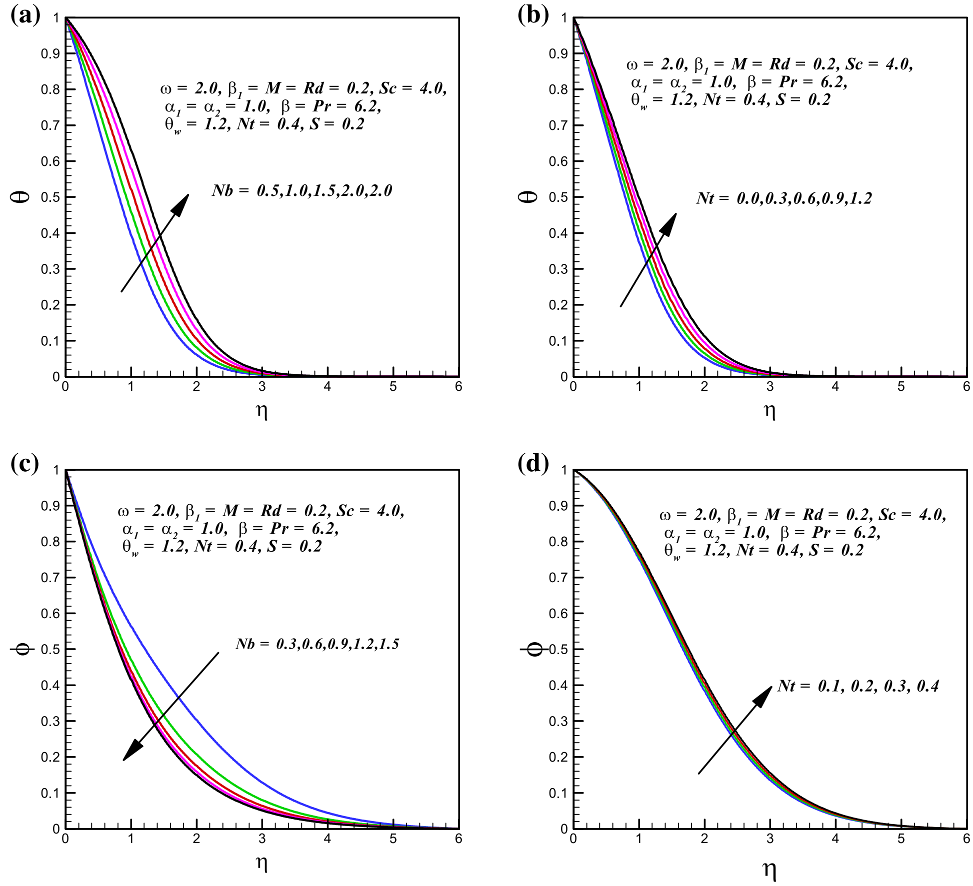

Fig. 5 Variation of Nt and Nb on (**a**, **b**) temperature profile and (**c**, **d**) concentration profile

- The behavior of wall upward and downward motion parameter is observed similarly to that of injection and suction parameters.
- Overall the impact of wall motion parameter on radial, azimuthal, axial velocities, temperature and concentration profiles is to enhanced, these.
- Temperature profile of nanofluid is enhanced, while concentration field reduces with higher values of Brownian motion.
- Boundary layer of both thermal and concentration profiles is enhanced due to increasing thermophoresis effects.
- Magnetic field effects are observed to reduce the radial and azimuthal velocity of nanofluid.
- Nusselt number is increased by decreasing the values of wall motion parameter.

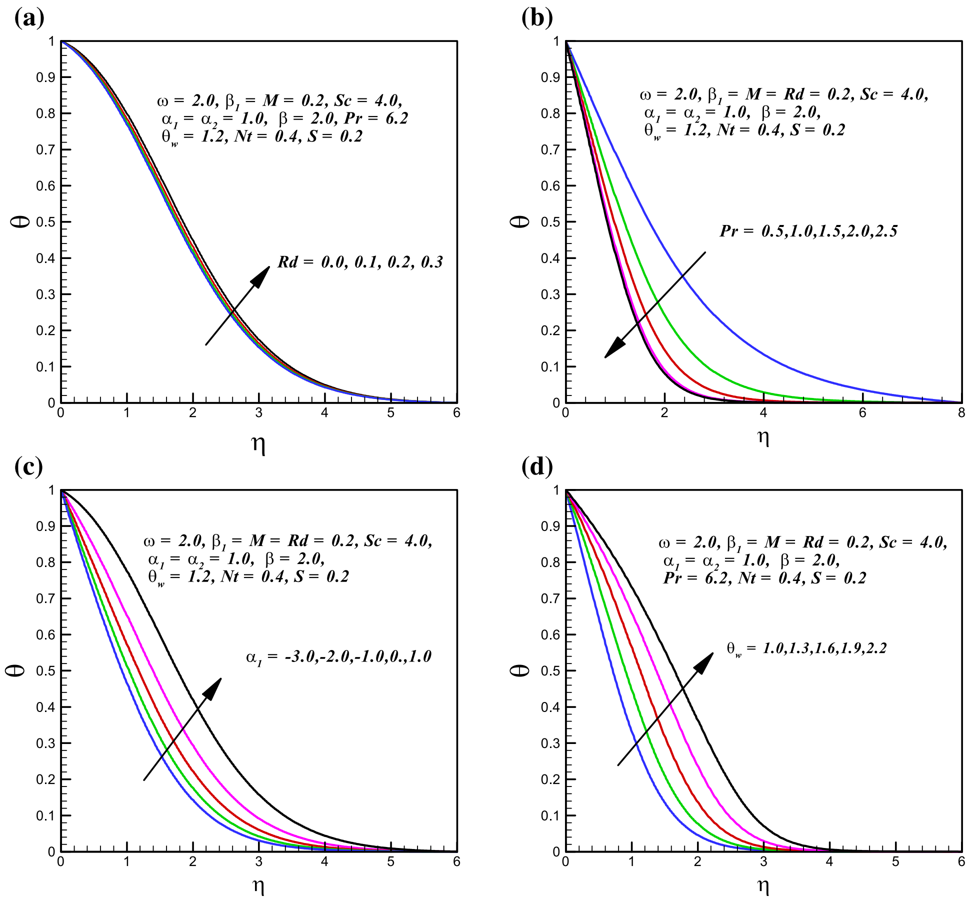

Fig. 6 Variation of **a** Rd, **b** Pr, **c** α_1 and **d** θ_w on temperature profile

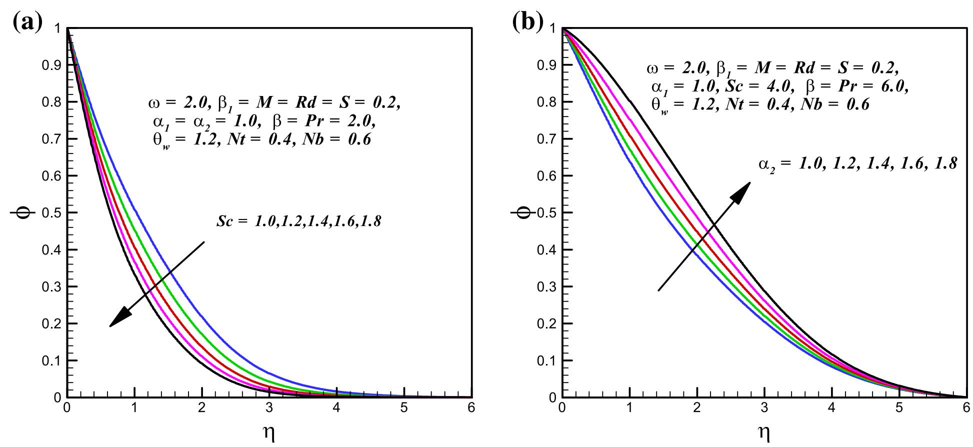

Fig. 7 Variation of concentration profile ϕ with **a** Sc, **b** α_2

Fig. 8 Nusselt number for **a** Nt, Nb **b** Rd, ω, and Sherwood number for **c** S, Nb **d** Nt, Nb

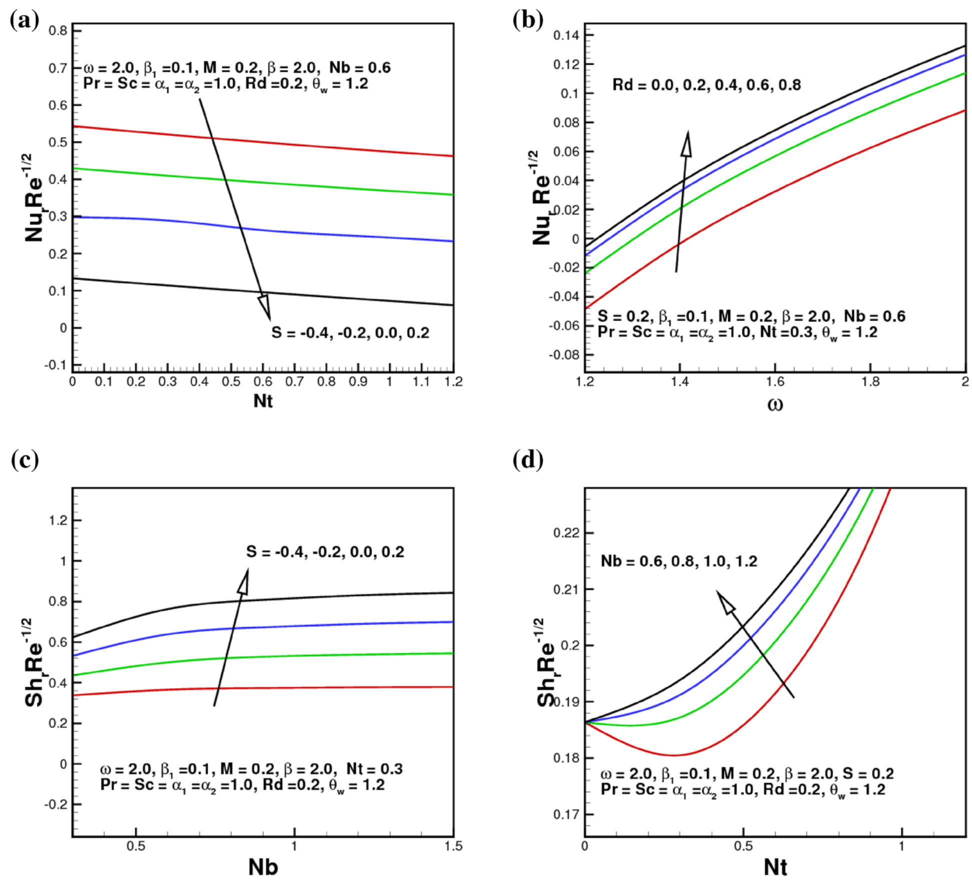

Table 1 A comparison of $F'(0)$, $G'(0)$ and $-\theta'(0)$ for various values of S when $\omega = 1.0$

		$S=-0.3$	$S=-0.2$	$S=0.0$	$S=0.5$	$S=1.0$	$S=2.0$
$F'(0)$	Ref. Turkyilmazoglu (2018)	0.4441589	0.4655632	0.5102326	0.6282715	0.7523955	1.0081383
$F'(0)$	Present	0.4441004	0.4545134	0.5101162	0.6282694	0.7480302	1.0072935
$G'(0)$	Ref. Turkyilmazoglu (2018)	− 0.7909736	− 0.7320534	− 0.6159220	− 0.3351635	− 0.0691935	0.4168670
$G'(0)$	Present	− 0.7908021	− 0.7319906	− 0.6158492	0.3351622	− 0.0675794	0.4169216
$-\theta'(0)$	Ref. Turkyilmazoglu (2018)	0.4968173	0.4585096	0.3962475	0.2543630	0.1221723	− 0.1172784
$-\theta'(0)$	Present	0.4969023	0.4588884	0.3962613	0.2549728	0.1223241	− 0.1174905

Table 2 A comparison of $F'(0)$, $G'(0)$ and $-\theta'(0)$ for various values of S when $\omega = 2.0$

		$S=-0.3$	$S=-0.2$	$S=0.0$	$S=0.5$	$S=1.0$	$S=2.0$
$F'(0)$	Ref. Turkyilmazoglu (2018)	1.3433822	1.3764212	1.4431558	1.6124395	1.7830279	2.1192174
$F'(0)$	Present	1.3433487	1.3763832	1.4431391	1.6125125	1.7798691	2.1184254
$G'(0)$	Ref. Turkyilmazoglu (2018)	− 2.0262846	− 1.9307068	− 1.7420905	− 1.2855033	− 0.8504318	− 0.0438094
$G'(0)$	Present	− 2.0261303	− 1.9305345	− 1.7420796	− 1.2854845	− 0.8494254	− 0.0437268
$-\theta'(0)$	Ref. Turkyilmazoglu (2018)	0.6480313	0.6180882	0.5603786	0.4221667	0.2918228	0.0528206
$-\theta'(0)$	Present	0.6487922	0.6185145	0.5604118	0.4221667	0.2919746	0.0525969

Acknowledgements This work has the financial supports from Higher Education Commission (HEC) of Pakistan under the project number: 6210.

References

Ahmed J, Khan M, Ahmad L (2019) Transient thin film flow of nonlinear radiative Maxwell nanofluid over a rotating disk. Phys Lett A 383(12):1300–1305

Ahmed J, Khan M, Ahmad L (2019) Stagnation point flow of Maxwell nanofluid over a permeable rotating disk with heat source/sink. J Mol Liq 287:110853

Ahmed J, Khan M, Ahmad L (2019) Transient thin-film spin-coating flow of chemically reactive and radiative Maxwell nanofluid over a rotating disk. Appl Phys A 125(3):125–161

Ahmed J, Khan M, Ahmad L (2019) Swirling flow of Maxwell nanofluid between two coaxially rotating disks with variable thermal conductivity. J Braz Soc Mech Sci Eng 41(2):41–97

Akbar NS, Raza M, Ellahi R (2016) Impulsion of induced magnetic field for brownian motion of nanoparticles in peristalsis. Appl Nanosci 6(3):359–370

Alamri SZ, Ellahi R, Shehzad N, Zeeshan A (2019) Convective radiative plane Poiseuille flow of nanofluid through porous medium with slip: an application of Stefan blowing. J Mol Liq 273:292–304

Alebraheem J, Ramzan M (2019) Flow of nanofluid with Cattaneo-Christov heat flux model. Appl Nanosci. https://doi.org/10.1007/s13204-019-01051-z

Anwar OA, Mabood F, Islam MN (2015) Homotopy simulation of nonlinear unsteady rotating nanofluid flow from a spinning body. Int J Eng Math 15. ID 272079

Avramenko AA, Blinov DG, Shevchuk IV (2014) Self-similar analysis of fluid flow and heat-mass transfer of nanofluids in boundary layer. Phys Fluids 23(8):082002

Bird RB, Armstrong RC, Hassager O (1977) Dynamics of polymeric liquids fluid mechanics, vol 1. Wiley, New York

Buongiorno J (2006) Convective transport in nanofluids. ASME J Heat Transf 128(3):240–250

Choi SUS, Eastman JA (1995) Enhancing thermal conductivity of fluids with nanoparticles. ASME I Mech Eng Congr 66:99–105

Chon CH, Kihm KD (2005) Thermal conductivity enhancement of nanofluids by Brownian motion. J Heat Tranf 127(8):810

Das SK, Putra N, Thiesen P, Roetzel W (2003) Temperature dependence of thermal conductivity enhancement for nanofluids. J Heat Transf 125:567–574

Ellahi R, Hassan M, Zeeshan A, Khan AA (2016) The shape effects of nanoparticles suspended in HFE-7100 over wedge with entropy generation and mixed convection. Appl Nanosci 6(5):641–651

Ellahi R, Hussain F, Abbas SA, Sarafraz MM, Goodarzi M, Shadloo MS (2020) Study of two-phase newtonian nanofluid flow hybrid with hafnium particles under the effects of slip. Inventions 5(1):6

Ellahi R, Sait SM, Shehzad N, Mobin N (2019) Numerical simulation and mathematical modeling of electro-osmotic Couette-Poiseuille flow of MHD power-law nanofluid with entropy generation. Symmetry 11(8):1038

Ezzat MA (2010) Thermoelectric MHD non-Newtonian fluid with fractional derivative heat transfer. Phy B Cond Matt 405(19):4188–4194

Hall P (1986) An asymptotic investigation of the stationary modes of instability of the boundary layer on a rotating disc. Proc R Soc Lond A 406(1830):93–106

Hatami M, Ganji DD (2014) Natural convection of sodium alginate non-Newtonian nanofluid flow between two vertical flat plates by analytical and numerical methods. Case Stud Ther Eng 2:14–22

Hayat T, Ahmad S, Khan MI, Alsaedi A (2018) Modeling chemically reactive flow of sutterby nanofluid by a rotating disk in presence of heat generation/absorption. Comm Theor Phys 69(5):569

Hayat T, Imtiaz M, Alsaedi A, Kutbi MA (2015) MHD three-dimensional flow of nanofluid with velocity slip and nonlinear thermal radiation. J Magn Magn Mater 396:31–37

Hayat T, Muhammad T, Alsaedi A, Alhuthali MS (2015) Magnetohydrodynamic three-dimensional flow of viscoelastic nanofluid in the presence of nonlinear thermal radiation. J Mag Mag Mater 385:222–229

Hayat T, Shafique M, Tanveer A, Alsaedi A (2016) Hall and ion slip effects on peristaltic flow of Jeffrey nanofluid with joule heating. J Magn Magn Mater 407:51–59

Hossain MA, Alim MA, Rees DA (1999) The effect of radiation on free convection from a porous vertical plate. Int J Heat Mass Transf 42:181–191

Jarre S, Le Gal P, Chauve MP (1996) Experimental study of rotating disk instability, I. Natural flow. Phys Fluids 8(2):496–508

Karman TV (1921) Uber laminare und turbulente reibung. J Appl Math Mech 1:233–252

Khan M, Ahmed J, Ali W (2020) Thermal analysis for radiative flow of magnetized Maxwell fluid over a vertically moving rotating disk. J Therm Anal Calorim. https://doi.org/10.1007/s10973-020-09322-6

Khan JA, Mustafa M, Hayat T, Alsaedi AA (2018) Revised model to study the MHD nanofluid flow and heat transfer due to rotating disk: numerical solutions. Neural Compt Appl 30(3):957–964

Khan JA, Mustafa M, Hayat T, Farooq MA, Alsaedi A, Liao SJ (2014) On model for three-dimensional flow of nanofluid an application to solar energy. J Mol Liq 194:41–47

Khan M, Ahmed J, Ali W (2020) An improved heat conduction analysis in swirling viscoelastic fluid with homogeneous-heterogeneous reactions. J Therm Anal Calorim https://doi.org/10.1007/s10973-020-09342-2

Kuiken HK (1971) The effect of normal blowing on the flow near a rotating disk of infinite extent. J Fluid Mech 47:789–798

Li CH, Peterson GP (2006) Experimental investigation of temperature and volume fraction variations on the effective thermal conductivity of nanoparticle suspensions. J Appl Phys 99(8):084314

Mustafa M (2017) MHD nanofluid flow over a rotating disk with partial slip effects: buongiorno model. Int J Heat Mass Transf 108:1910–1916

Nadeem S, Haq RU, Khan ZH (2014) Numerical solution of non-Newtonian nanofluid flow over a stretching sheet. Appl Nanosci 4(5):625–631

Owen JM, Haynes CM, Bayley FJ (1974) Heat transfer from an air-cooled rotating disk. Proc R Soc Lond A 336(1607):453–473

Peng Y, Lv BH, Yuan JL, Ji HB, Sun L, Dong CC (2014) Application and prospect of the non-Newtonian fluid in industrial field. Mat Sci Forum 770:396–401

Sarafraz MM, Pourmehran O, Yang B, Arjomandi M, Ellahi R (2020) Pool boiling heat transfer characteristics of iron oxide nano-suspension under constant magnetic field. Int J Therm Sci 147:106131

Sheikholeslami M, Ellahi R, Ashorynejad HR, Domairry G, Hayat T (2014) Effects of heat transfer in flow of nanofluids over a permeable stretching wall in a porous medium. J Compt Theort Nanosci 11(2):486–496

Sheikholeslami M, Ganji DD, Rashidi MM (2016) Magnetic field effect on unsteady nanofluid flow and heat transfer using Buongiorno model. J Mag Magn Mater 416:164–173

Stuart JT (1954) On the effects of uniform suction on the steady flow due to a rotating disk. Q J Mech Appl Math 7(4):446–456

Turkyilmazoglu M (2014) Nanofluid flow and heat transfer due to a rotating disk. Comput Fluids 94:139–146

Turkyilmazoglu M (2016) Flow and heat simultaneously induced by two stretchable rotating disks. Phys Fluids 28(4):043601

Turkyilmazoglu M (2018) Fluid flow and heat transfer over a rotating and vertically moving disk. Phys Fluid 30(6):063605

Turkyilmazoglu M (2019) Free and circular jets cooled by single phase nanofluids. Eur J Mech-B/Fluids 76:1–6

Turkyilmazoglu M (2019) Fully developed slip flow in a concentric annuli via single and dual phase nanofluids models. Comput Method Programs Biomed 179:104997

Turkyilmazoglu M (2020) Single phase nanofluids in fluid mechanics and their hydrodynamic linear stability analysis. Comput Method Program Biomed 187:105171